Research Article | Vol. 27, No. 21 / 14 October 2019 / Optics Express 29949
Optics EXPRESS

Incoherent phonon population and exciton-exciton annihilation dynamics in monolayer WS_2 revealed by time-resolved Resonance Raman scattering

SHUANGPING HAN,[1,3] CHRISTOPH BOGUSCHEWSKI,[2] YAN GAO,[1,3,4] LIANTUAN XIAO,[1,3] JINGYI ZHU,[2] AND PAUL H. M. VAN LOOSDRECHT[2,5]

[1]*State Key Laboratory of Quantum Optics and Quantum Optics Devices, Institute of Laser Spectroscopy, Shanxi University, Taiyuan, Shanxi 030006, China*
[2]*Physics institute 2, University of Cologne, 50937, Germany*
[3]*Collaborative Innovation Center of Extreme Optics, Shanxi University, Taiyuan, Shanxi 030006, China*
[4]*ago@sxu.edu.cn*
[5]*pvl@ph2.uni-koeln.de*

Abstract: Atomically thin layer transition metal dichalcogenides have been intensively investigated for their rich optical properties and potential applications on nano-electronics. In this work, we study the incoherent phonon and exciton population dynamics in monolayer WS_2 by time-resolved Resonance Raman scattering spectroscopy. Upon excitation of the exciton transition, both Stokes and anti-Stokes scattering strength of the optical and the longitudinal acoustic two phonon modes exhibit large reduction. Based on the assumption of quasi-equilibrium distribution, the hidden phonon population dynamics is retrieved, which shows an instant build-up and a relaxation lifetime of ~4 ps at the exciton density $\sim 10^{12}\mathrm{cm}^{-2}$. A phonon temperature rises of ~20 K was identified due to the exciton excitation and relaxation. The exciton relaxation dynamics extracted from the transient vibrational Raman response shows strong excitation density dependence, signaling an important bi-molecular contribution to the decay. These results provide significant knowledge on the thermal dynamics after optical excitation, enhance the understanding of the fundamental exciton dynamics in two-dimensional transition metal materials, and demonstrate that time-resolved Resonance Raman scattering spectroscopy is a powerful method for exploring quasi-particle dynamics in optical materials.

1. Introduction

While the rise of graphene materials [1] and their researches are still booming, various other atomically thin materials have emerged, sparking a novel and fascinating field of research [2,3]. Among them, monolayer transition metal dichalcogenides (TMDCs) play an important role, arising from the intriguing physical properties rooted in their reduced dimensionality and lack of inversion symmetry. TMDCs are regarded by many as a new generation of functional materials with a strong potential for applications in optoelectronic devices [4–9].

One of the significant differences between monolayer TMDCs and graphene is that the former shows an intrinsic bandgap, with transition energies ranging from visible to near infrared frequencies. Rather than free carrier excitations, the lowest energy electronic excitations are strongly bound electron-hole pairs, i.e. excitons with large binding energies up to a few hundred meV [10–13]. These excitonic transitions provide an ideal platform for the study of exciton properties and the related optical induced relaxation dynamics in two dimensional semiconductors. This is not only of strong interest from a fundamental materials science point of view, but is

#371833 https://doi.org/10.1364/OE.27.029949
Journal © 2019 Received 4 Jul 2019; revised 15 Aug 2019; accepted 18 Aug 2019; published 2 Oct 2019

Optics EXPRESS

also pivotal in eventually realizing the application potential of TMDCs. Not surprisingly, the properties induced by optical excitation and the associated relaxation dynamics in TMDCs have been extensively studied in the recent past with various ultrafast spectroscopic techniques [14–25]. These studies revealed a number of interesting properties, including a giant optically induced band gap renormalization [19,20,25] leading to a pronounced spectral dynamics, a strong valley-selective optical Stark effect [26–28], which is of interest in view of optical control in possible valleytronics applications, and a strong material and excitation dependence of the exciton relaxation dynamics showing timescales ranging from tens to hundreds of picoseconds originating from both first and second order relaxation processes [16,18,21,22,24].

Whereas previous ultrafast spectroscopic studies on monolayer TMDCs mainly focused on the electronic excitation aspects, the lattice and thus the phonon population dynamics, which play a crucial role in the energy dissipation after optical excitation, have not yet been investigated in a direct manner [29]. Time-resolved Resonance Raman spectroscopy (TRSRS) can provide a direct access to study both the incoherent phonon relaxation as well as the electron-phonon coupling dynamics [30–34]. Recently we have demonstrated that not only the phonons but also the exciton population dynamics can be detected by monitoring the optical induced differential Stokes and anti-Stokes Raman signals in one-dimensional graphene nanoribbons [35]. Especially, under a strongly resonant condition, the exciton dynamics can be directly obtained from the differential Stokes signal due to its relatively weak dependence on the induced changes in the phonon population. Here we report on an investigation of the phonon creation and relaxation dynamics as well as the exciton relaxation and annihilation mechanisms in monolayer WS_2 using TRSRS. The observed fast phonon population and depopulation dynamics show an efficient electron-lattice and phonon-phonon coupling leading to fast initial energy dissipation after optical excitation. The observed exciton relaxation time depends strongly on the intensity of the initial excitation, demonstrating that exciton-exciton annihilation contributes strongly to the exciton relaxation dynamics in monolayer WS_2.

2. Experimental methods

Monolayer WS_2 samples were produced through chemical vapour deposition (CVD) [36,37] on a thick oxide coated (280 nm) silicon substrate. The sample was characterized using atomic force microscopy (AFM), steady state photoluminescence and Raman spectroscopy. The steady state Raman and photoluminescence spectra were recorded using a micro-Raman setup equipped with a triple stage spectrometer (Spectroscopy & Imaging GmbH) and liquid nitrogen cooled (−120 °C) CCD detector (PyLoN 100; Princeton Instruments). A picosecond laser (515 nm, ~ 2ps) was used for the standard Raman and luminescence measurements. The 515 nm laser pulse was spectrally cleaned and narrowed (full width a half maximum (FWHM) ~10 cm^{-1}) using a home build pulse shaper. The laser pulses were focused on the sample using microscope objective (20×, NA = 0.4). Raman and photoluminescence signals of WS_2 were collected in a backscattering geometry.

Details of the TRSRS technique used here and related data analysis methods have been described elsewhere [38]. Briefly, an integrated ultrafast laser system (Light Conversion PHAROS) with two outputs of the fundamental pulses (300 fs and 150 ps, @1030 nm) pump two optical parametric amplifiers (Light Conversion), one to generate laser pulses for selective excitation (~300 fs), and one to generate a narrow-bandwidth laser pulse for Raman probing(~2 ps). For excitation of the WS_2 sample, the pump pulse wavelength was centered at ~ 620 nm (2.0 eV), corresponding to the direct A exciton resonance. The Raman probe pulse was set at 515 nm (2.4 eV), in resonance with the B excitonic transition [12]. This configuration of pump and probe yields a strong resonant Raman probing signal and a direct excitation of excitons with only a small amount of excess energy. In order to minimize the background scattering induced by the relatively strong pump

Optics EXPRESS

pulse, a crossed linear polarization of pump and probe was used, while detecting the Raman signal polarized parallel to the probe pulse.

3. Results and discussion

The inset of Fig. 1(a) shows an optical image of the triangular crystalline monolayer WS_2 sample. The main panel 1(a) presents an AFM line scan along the dashed line in the inset image, showing the for a monolayer expected thickness of roughly 0.8 nm [39]. The monolayer quality of the sample was further confirmed by the steady state photoluminescence (PL) and Raman spectra presented in Fig. 1(b) and 1(c), respectively. The PL spectrum has a peak located around 1.97 eV, corresponding to the excitonic A transition of crystalline single layer WS_2 [39,40]. The Raman spectrum shows a strong response at 350 cm^{-1}, which is generally considered to be contributed by a mixture of E_{2g} and 2LA modes, however under the Raman probing wavelength at ~515 nm, the 2LA signal dominates [41,42]. A relatively weaker peak at 415 cm^{-1} corresponding to the A_{1g} mode originating from the out-of-plane vibration of sulfur atoms [43–45]. The peak located at 520 cm^{-1} is due to the underlying silica/silicon substrate. The peak positions and the relative ratio of peak intensities are in good agreement with previously reported Raman spectra of monolayer WS_2 on silica/silicon substrate [42,46].

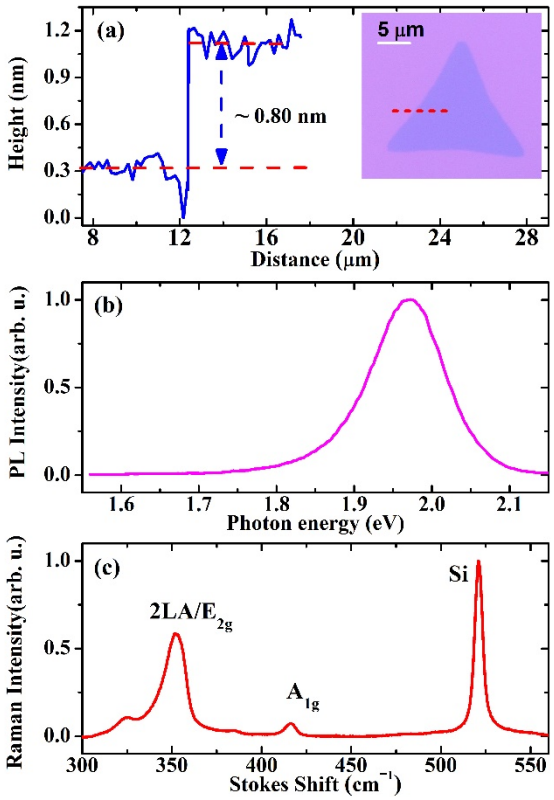

Fig. 1. Steady state spectra characterization of the CVD grown monolayer WS_2 sample on silica/silicon substrate. (a) Atomic force microscope (AFM) measurement the thickness of monolayer WS_2, inset show the optical image and AFM scanning range (dashed red line). (b) Photoluminescence. (c) Steady Raman scattering.

Time-resolved Resonance Raman scattering spectra of monolayer WS_2 are presented in Fig. 2. In Fig. 2(a), it shows the transient Stokes and anti-Stokes spectra for various pump-probe delay

Optics EXPRESS

times using an initial photo-excited exciton density around 2.26×10^{12} cm^{-2}, whereas in Fig. 2(b) it shows the derived difference spectra obtained by subtracting the response at −5 ps. From these spectra it is clear that the optical pump induces a significant reduction of the scattering efficiency of all phonon modes, without any spectral dynamics of broadening or shifting, which recovers on a time scale of tens of ps. As we have discussed previously for the resonant Raman scattering case [35] the induced transient changes may originate both from changes in the resonant enhancement due to electronic population effects (typically leading to a reduction of the response) as well as from changes in the vibrational population (typically leading to an increase of the response). Normally semiconductors show an induced increase of the anti-Stokes Raman signals [30,31,33–35,47,48] assigned to a dominated contribution of optical phonon populations, and an increase or decrease of the Stokes scattering depending on resonance conditions. For monolayer WS_2, however, this is not the case. Here both Stokes and anti-Stokes scattering show a transient decrease. This indicates the optically induced phonon population contribution, which would give an enhanced Raman response, is extremely small, and the transient changes in the Raman response is primarily due to state filling effects which suppress the Resonance behavior of the response.

To obtain a better view on the detailed relaxation dynamics of the optical phonon scattering, the strongest signal from 2LA/E_{2g} phonon peak at ~ 350 cm^{-1} was spectrally integrated (red bar indicated area in Fig. 2(a) for different delay times. The obtained decay dynamics are presented in Fig. 3 for the Stokes 3(a) and anti-Stokes 3(b) responses. Though both anti-Stokes and Stokes sides show a transient reduction with a recovery time of some 10s of ps, the detailed transient response is substantially different, in particular at early times. The origin of this difference is the (positive) contribution of the phonon population to the response, in particular for the anti-Stokes signal. In order to retrieve the phonon population dynamics and lattice temperature, we assume the signal ~ 350 cm^{-1} are mostly contributed by the dominated 2LA modes, ignoring the smaller part of E_{2g}, and after excitation quasi-equilibrium between electron-phonon are immediately (in less than 1 ps) built. For Stokes side, the Raman signal (I_S) of 2LA phonon can be expressed (see Appendix A) as:

$$I_S \propto 2(1+n)^2, \tag{1}$$

where

$$n = 1/[exp(h\Omega/k_BT) - 1], \tag{2}$$

is the statistically averaged phonon population number. And in Eq. (2) h is Planck constant, Ω is the optical phonon frequency, k_B is the Boltzmann constant and T is the phonon temperature. Similarly, anti-Stokes side (I_{AS}) Raman signal of two phonon transition can be obtained (see Appendix A) as:

$$I_{AS} \propto 2n^2 \tag{3}$$

We further make the assumption that before time zero, the phonon temperature is close to the Room temperature (300 K) and the two phonon transition Raman polarizability matrix elements is not changing after excitation. These assumption are reasonable in view of the low Raman probe laser pulse fluence, and the observation that there are no significant differences between pre-zero delay time intensities measured with and without the presence of the pump laser beam. By using Eqs. (1)–(3) and above assumption, time dependent phonon temperature can be readily extracted by using the measured Stokes and anti-Stokes signals.

The transient phonon temperature determined using Eqs. (1)–(3) presented in Fig. 3(c) shows an instantaneous (within our time resolution) increase by about 22 K, corresponding to a transient increase of the LA phonon population. The increased phonon relaxes with a decay time of 4.3 ps to a long lived quasi equilibrium state with a temperature of about 3 K above base temperature, which further relaxes to the base temperature outside our detection time window but within the time between two pump pulses (10 μs). Similarly, the one phonon temperature from the

Optics EXPRESS

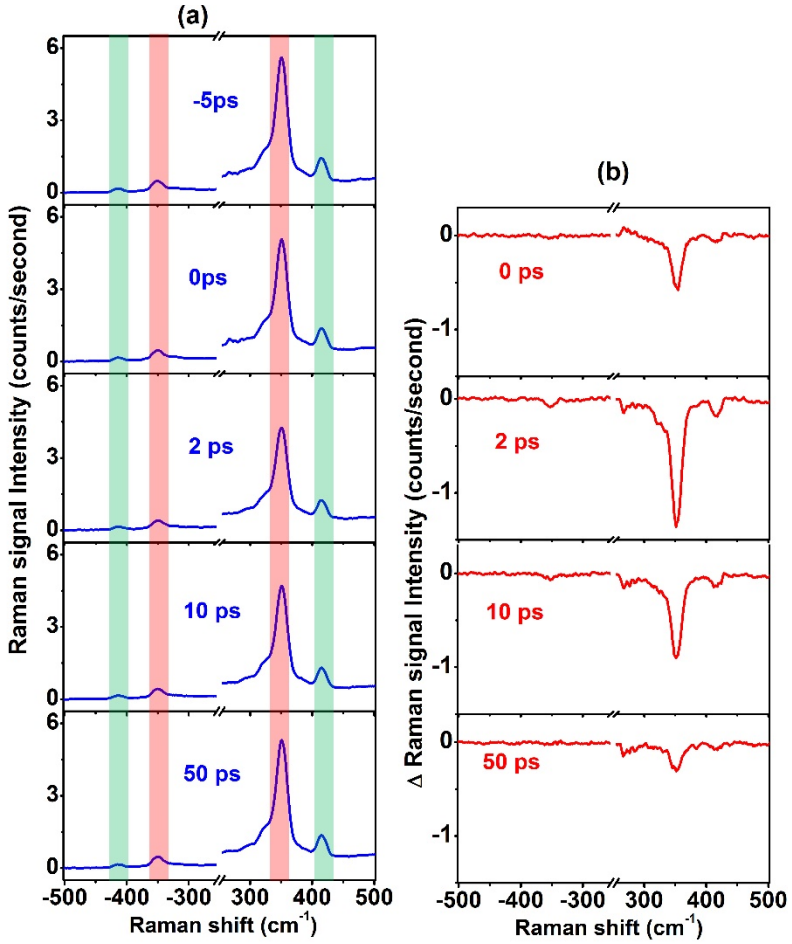

Fig. 2. Time-resolved Resonance Raman scattering spectra of the monolayer WS_2 on silica/silicon recorded on both Stokes and anti-Stokes sides simultaneously. (a) Raman scattering intensity spectra at different delay times after optical pump at 2.0 eV (620 nm). (b) Pump induced difference spectra obtained by subtraction the spectrum at −5 ps from each spectrum in (a) at different corresponding delay times.

Optics EXPRESS

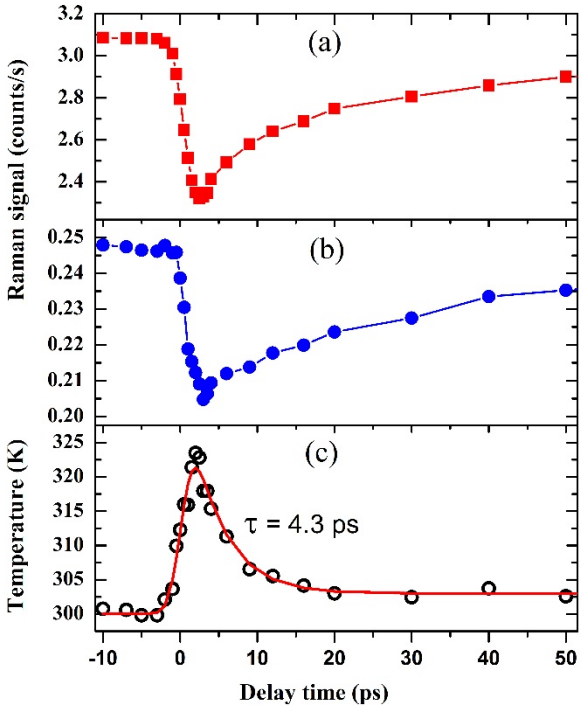

Fig. 3. Decay dynamics of the optical phonon peak at around 350 cm^{-1} at the exciton density around 2.26×10^{12} cm^{-2}. (a) Stokes side dynamics integrated in the spectral region from 338 to 362 cm^{-1}. (b) Anti-Stokes side dynamics integrated in the spectral region from −362 to −338 cm^{-1}. (c) Calculated temperature of the optical phonon according to Bose-Einstein statistics.

A_{1g} modes at ~415 cm^{-1} (green bar indicated area in Fig. 2(a) can be calculated by using the corresponding equations for the one phonon case, and similar temperature and decay dynamics were obtained (see Appendix B) in the error range of our experiments.

The observation of the fast (<2ps) rise in phonon temperature after excitation suggests that phonon populations are created through a fast exciton-phonon scattering process. This can be either through release of the excess energy of the optically excited exciton states, or through transitions from the optically excited bright exciton states into optically inactive dark exciton states. In monolayer WS_2 the dark exciton state is formed by the electrons in the conduction band and holes in the valence band with opposite spins, and the energy of this dark exciton state is slightly lower than the bright exciton state [49–53]. Since relaxation from the bright to the dark exciton state requires a spin flip of the electrons, this process [54] is expected to be slower than the exciton cooling process but cannot be excluded on the basis of the current experiments. The relaxation of the 2LA and A_{1g} phonon population (~ 4 ps) can be ascribed to their scattering into lower acoustic phonon modes in the monolayer sample.

Apart from information on the phonon population dynamics and lattice temperature, one can straightforwardly derive the exciton population dynamics from the resonant TRSRS experiment. This is done by analyzing the time resolved optical phonon Stokes scattering signal, which is hardly influenced by the minor changes in total phonon population induced by the pump pulse. [35,38] The observed transient changes in the Stokes response can be ascribed to changes in the resonance enhancement due to ground state bleaching/excited state filling by the pump pulse, i.e. due to a transient reduction of the optical transition probability. The 10s of ps recovery time

Optics EXPRESS

of the phonon signals on Stokes side is therefore assigned to relaxation of the excited excitonic states. In order to get a better insight into the exciton relaxation dynamics we performed a set of experiments on Stokes side for varying initial exciton densities. Figure 4a shows the integrated 2LA mode Stokes side signal for different excitation densities. The data show a clear speed up of the recovery dynamics upon increasing excitation density, indicating that many body annihilation processes play a role in the decay dynamics.

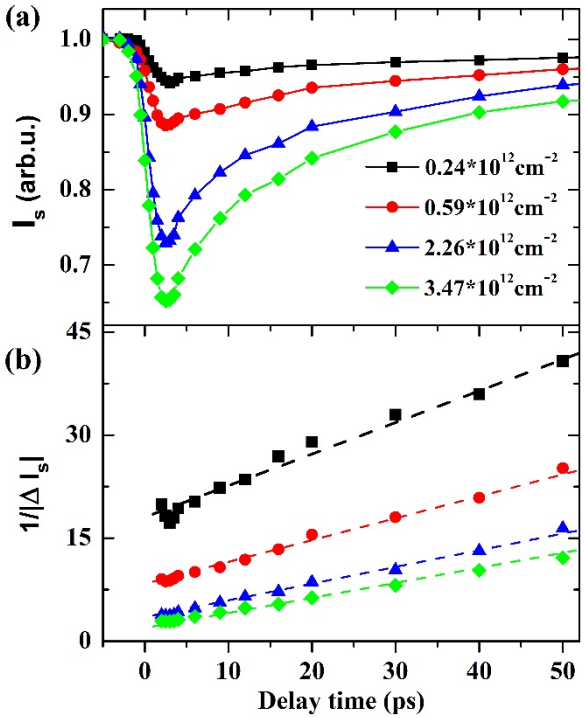

Fig. 4. Intensity dependence of the dynamics observed on Stokes side. (a) Decay dynamics of the 2LA phonon peak at around 350 cm^{-1} at different exciton density. (b) Inversion of the decay dynamics (dots) from (a) and the global fitted ones (dashed lines) with rate equation including both the first and second order exciton annihilation reaction (details see text in the paper). The global fitting extracted rate constants of $k_1 \sim (67\ ps)^{-1}$ and $k_2 \sim 0.104\ cm^2 s^{-1}$.

To analyse the observed phenomena, we model the dynamics by including both a first order free exciton decay process and a second order relaxation process, i.e., exciton-exciton annihilation. The population decay can then be expressed as:

$$dN(t)/dt = -k_1 N(t) - k_2 N_2(t), \tag{4}$$

where N(t) is the time dependent exciton population density, and k_1 (k_2) is the first (second) order rate constant. Analytically solving Eq. (4) gives

$$1/N(t) = [1/N(0) + k_2/k_1]exp(k_1 t) - k_2/k_1, \tag{5}$$

in which N(0) is the initially excited exciton density. Since the effective lifetime from the first order reaction is usually much longer than that from the second order one, to simplify the

Optics EXPRESS

description, in short time range, we expand $\exp(k_1 t)$ to $1 + k_1 t$ and Eq. (5) becomes:

$$1/N(t) \approx 1/N(0) + [k_1/N(0) + k_2]t \tag{6}$$

Expression Eq. (6) gives a very compact and intuitive description for the observed signals: it indicates that the inverse of the population should be simply linearly proportional to the delay time t, while the slope is excitation density dependent. Indeed, as shown in Fig. 4(b), this is exactly the case as indicated by the inverse of the differential Raman signals. Global fitting (dashed lines) of the data (symbols) using Expression Eq. (6) yields satisfactory agreement and a first order rate constant $k_1 = (67\ \text{ps})^{-1}$ and second order $k_2 = 0.104\ \text{cm}^2\text{s}^{-1}$. These values are comparable to those reported for other measurements on CVD grown monolayer WS_2 samples [21,22], confirming the importance of an efficient exciton-exciton annihilation process in monolayer WS_2. The slight difference of the rate constants observed here and those in previous experiments on CVD grown samples are most likely due to variations in defect densities. In particular we note that the values reported for CVD grown samples differ substantially from those measured on exfoliated samples. In exfoliated monolayer WS_2, the first order exciton decay rate constant was measured to be around $(806\ \text{ps})^{-1}$, one order slower, while the exciton-exciton annihilation rate k_2 was around $0.41\ \text{cm}^2\text{s}^{-1}$, 4 times larger [18]. Since the defect density ($\sim 3\times10^{13}\ \text{cm}^{-2}$) [55] in a usual CVD grown samples is usually much higher than that in exfoliated samples ($\sim 2\times10^{9}\ \text{cm}^{-2}$) [56], a huge difference which could strongly influences the diffusion of excitons [57] and thus affects both the first and second order decay processes, leading to a larger k_1 due to defect assisted recombination [58,59] and a smaller k_2 due to slower diffusion in CVD grown WS_2. These results suggest that the quantum efficiency of light emission and thermal effects caused by strong excitation conditions may be optimized for optical device applications by manipulating the defects density in the fabrication process of TMDCs.

4. Conclusions

In conclusion we have investigated the relaxation dynamics induced by optical excitation of both the phonons and excitons in the CVD grown monolayer WS_2 using TRSRS spectroscopy. The population of the optical and 2LA phonon show a very fast (<2ps) increase due to exciton-phonon coupling after optically inducing an exciton population. The higher frequency phonon population decays with time constant of around 4 ps through phonon-phonon scattering. The exciton relaxation and annihilation dynamics, as observed through the time dependent Stokes optical phonon signals show the presence of both first and second order decay processes. Specific modelling of the observed dynamics obtained the first order and the second order exciton decay rates which are consistent with those obtained by other methods for CVD grown samples, but differ substantially from those for exfoliated samples due to the higher defect density. The present results provide a direct insight into both the excitonic and vibration energy dissipation properties of TMDC materials which has relevance to potential electro-optical TMDC applications, in particular under strong optical or electronic excitation conditions.

Appendix A: Two phonon transition in Raman scattering

To simplify the description and get intuitive into the two phonon scattering process, we use semi-classic theory of Raman scattering, by considering Raman scattering signal as originating from a change in local polarizability due to the presence of vibrational modes in the system.

For an applied electromagnetic filed $E(\omega)$, a polarization is induced :

$$P(\omega) = \chi E(\omega) \tag{7}$$

which acts as a source of the scattering light emission. Here χ is the macroscopic electronic tensor. Grafting into quantum mechanics, it is the transition probability square which determines

Optics EXPRESS

the Raman signal (I^R),

$$I^R \propto |<f|\chi|i>|^2 \tag{8}$$

In which $|<i|$ and $|<f|$ are the total initial and final state of the system. Considering only one normal coordinates of the phonon (Q_k), expending χ as:

$$\chi = \chi_0 + (d\chi/dQ_k)_0 Q_k + (d^2\chi/dQ^2{}_k)_0 Q^2{}_k + \ldots \tag{9}$$

Apparently the third term in Eq. (9) gives the two phonon transition of Raman process. Considering random phonon number state v, for Stokes side two phonon Raman scattering process:

$$I^{2R}{}_S \propto |<v+2|Q^2{}_k|v>|^2 \propto 2 + 3v + v^2, \tag{10}$$

and for anti-Stokes side

$$I^{2R}{}_{AS} \propto |<v-2|Q^2{}_k|v>|^2 \propto v^2 - v. \tag{11}$$

Next step we further considering the quasi-thermal equilibrium situation, the occupation probability (η_v) of v phonon state in a thermal average is:

$$\eta_v = exp(-\varepsilon_v/k_BT)/\sum\nolimits_v exp(-\varepsilon_v/k_BT) = exp[-h\Omega(v+1/2)/k_BT]/\sum\nolimits_v exp[-h\Omega(v+1/2)/k_BT]. \tag{12}$$

Where h is the Planck constant, k_B is Boltzmann constant and Ω is the phonon frequency.

Thus, in thermal equilibrium,

$$I^{2R}{}_S \propto \sum\nolimits_v (2 + 3v + v^2)\eta_v \propto 2(1+n)^2, \tag{13}$$

and

$$I^{2R}{}_{AS} \propto \sum\nolimits_v (v^2 - v)\eta_v \propto 2n^2 \tag{14}$$

with n defined to be the thermal average phonon number, *i.e.*,

$$n = 1/[(exp(h\Omega/k_BT) - 1]. \tag{15}$$

From Eqs. (7) and (8) we have:

$$C * I^{2R}{}_S/I^{2R}{}_{AS} = (1+n)^2/n^2 = exp(2h\Omega/k_BT) \tag{16}$$

$I^{2R}{}_S$ and $I^{2R}{}_{AS}$ are from experimental measurements, therefore, using Eqs. (15) and (16), phonon population and the temperature can be estimated. The pre-factor C in Eq. (16) can be determined by assuming Room temperature (~300 K) before time zero, and and assume it does not change during all the delay time in experiments.

Appendix B: One phonon transition in Raman scattering

Similarly, one phonon Raman transition can be treated in the same way as above, the results are trivial [60,61] and have been known as:

$$I^{1R}{}_S \propto 1 + n \tag{17}$$

for Stokes side, and

$$I^{1R}{}_{AS} \propto n \tag{18}$$

for anti-Stokes side.

As for the single phonon mode A_{1g} in WS_2 at around 415 cm^{-1}, the time dependent Stokes and anti-Stokes scattering results and calculated temperature according to Eqs. (17) and (18) are presented in Fig. 5:

Optics EXPRESS

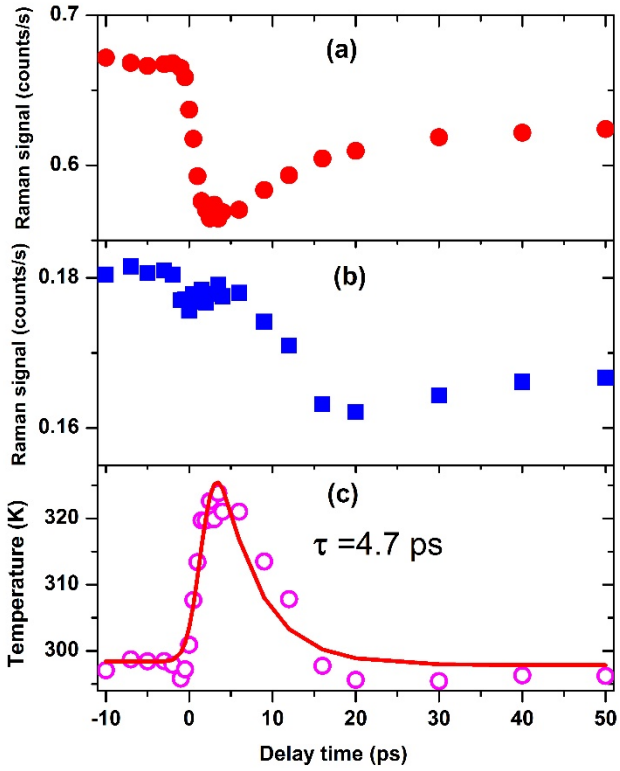

Fig. 5. Decay dynamics of the optical phonon peak at around 415 cm^{-1} at the exciton density around 2.26×10^{12} cm^{-2}. (a) Stokes side dynamics integrated in the spectral region from 400 to 430 cm^{-1}. (b) Anti-Stokes side dynamics integrated in the spectral region from −430 to −400 cm^{-1}. (c) Calculated temperature of the optical phonon according to Bose-Einstein statistics.

Funding

Deutsche Forschungsgemeinschaft (277146847, CRC 1238); National Natural Science Foundation of China (11434007, 61527824, 61605104); Program for Changjiang Scholars and Innovative Research Team in University (IRT_17R70); 111 Project (1331KSC, D18001); Shanxi Provincial Key Research and Development Project (2016021017, 2017YFA0304203).

References

1. K. S. Novoselov, "Electric field effect in atomically thin carbon films Science," Science **306**(5696), 666–669 (2004).
2. M. Ashton, J. Paul, S. B. Sinnott, and R. G. Hennig, "Topology-Scaling Identification of Layered Solids and Stable Exfoliated 2D Materials," Phys. Rev. Lett. **118**(10), 106101 (2017).
3. J. N. Coleman, M. Lotya, A. O'Neill, S. D. Bergin, P. J. King, U. Khan, K. Young, A. Gaucher, S. De, R. J. Smith, I. V. Shvets, S. K. Arora, G. Stanton, H. Y. Kim, K. Lee, G. T. Kim, G. S. Duesberg, T. Hallam, J. J. Boland, J. J. Wang, J. F. Donegan, J. C. Grunlan, G. Moriarty, A. Shmeliov, R. J. Nicholls, J. M. Perkins, E. M. Grieveson, K. Theuwissen, D. W. McComb, P. D. Nellist, and V. Nicolosi, "Two-dimensional nanosheets produced by liquid exfoliation of layered materials," Science **331**(6017), 568–571 (2011).
4. Q. H. Wang, K. Kalantar-Zadeh, A. Kis, J. N. Coleman, and M. S. Strano, "Electronics and optoelectronics of two-dimensional transition metal dichalcogenides," Nat. Nanotechnol. **7**(11), 699–712 (2012).
5. A. K. Geim and I. V. Grigorieva, "Van der Waals heterostructures," Nature **499**(7459), 419–425 (2013).
6. K. F. Mak and J. Shan, "Photonics and optoelectronics of 2D semiconductor transition metal dichalcogenides," Nat. Photonics **10**(4), 216–226 (2016).
7. F. Xia, H. Wang, D. Xiao, M. Dubey, and A. Ramasubramaniam, "Two-dimensional material nanophotonics," Nat. Photonics **8**(12), 899–907 (2014).

Optics EXPRESS

8. Q. Cao, Y. W. Dai, J. Xu, L. Chen, H. Zhu, Q. Q. Sun, and D. W. Zhang, "Realizing Stable p-Type Transporting in Two-Dimensional WS2 Films," ACS Appl. Mater. Interfaces **9**(21), 18215–18221 (2017).
9. A. S. Aji, P. Solís-Fernández, H. G. Ji, K. Fukuda, and H. Ago, "High Mobility WS2 Transistors Realized by Multilayer Graphene Electrodes and Application to High Responsivity Flexible Photodetectors," Adv. Funct. Mater. **27**(47), 1703448 (2017).
10. H.-P. Komsa and A. V. Krasheninnikov, "Effects of confinement and environment on the electronic structure and exciton binding energy of MoS2from first principles," Phys. Rev. B **86**(24), 241201 (2012).
11. A. Chernikov, T. C. Berkelbach, H. M. Hill, A. Rigosi, Y. Li, O. B. Aslan, D. R. Reichman, M. S. Hybertsen, and T. F. Heinz, "Exciton binding energy and nonhydrogenic Rydberg series in monolayer WS(2)," Phys. Rev. Lett. **113**(7), 076802 (2014).
12. C. X. Zhu B and X. Cui, "Exciton Binding Energy of Monolayer WS2," Sci. Rep. **5**(1), 9218 (2015).
13. S. Park, N. Mutz, T. Schultz, S. Blumstengel, A. Han, A. Aljarb, L.-J. Li, E. J. W. List-Kratochvil, P. Amsalem, and N. Koch, "Direct determination of monolayer MoS2 and WSe2 exciton binding energies on insulating and metallic substrates," 2D Mater. **5**(2), 025003 (2018).
14. P. J. Sim S and G. Song J, "Exciton dynamics in atomically thin MoS2 Interexcitonic interaction and broadening kinetics," Phys. Rev. B **88**(7), 075434 (2013).
15. T. Korn, S. Heydrich, M. Hirmer, J. Schmutzler, and C. Schüller, "Low-temperature photocarrier dynamics in monolayer MoS2," Appl. Phys. Lett. **99**(10), 102109 (2011).
16. D. Sun, Y. Rao, G. A. Reider, G. Chen, Y. You, L. Brezin, A. R. Harutyunyan, and T. F. Heinz, "Observation of rapid exciton-exciton annihilation in monolayer molybdenum disulfide," Nano Lett. **14**(10), 5625–5629 (2014).
17. A. Chernikov, C. Ruppert, H. M. Hill, A. F. Rigosi, and T. F. Heinz, "Population inversion and giant bandgap renormalization in atomically thin WS2 layers," Nat. Photonics **9**(7), 466–470 (2015).
18. L. Yuan and L. Huang, "Exciton dynamics and annihilation in WS2 2D semiconductors," Nanoscale **7**(16), 7402–7408 (2015).
19. E. A. Pogna, M. Marsili, D. De Fazio, S. Dal Conte, C. Manzoni, D. Sangalli, D. Yoon, A. Lombardo, A. C. Ferrari, A. Marini, G. Cerullo, and D. Prezzi, "Photo-Induced Bandgap Renormalization Governs the Ultrafast Response of Single-Layer MoS2," ACS Nano **10**(1), 1182–1188 (2016).
20. R. Schmidt, G. Berghauser, R. Schneider, M. Selig, P. Tonndorf, E. Malic, A. Knorr, S. Michaelis de Vasconcellos, and R. Bratschitsch, "Ultrafast Coulomb-Induced Intervalley Coupling in Atomically Thin WS2," Nano Lett. **16**(5), 2945–2950 (2016).
21. Y. Yu, Y. Yu, C. Xu, A. Barrette, K. Gundogdu, and L. Cao, "Fundamental limits of exciton-exciton annihilation for light emission in transition metal dichalcogenide monolayers," Phys. Rev. B **93**(20), 201111 (2016).
22. P. D. Cunningham, K. M. McCreary, and B. T. Jonker, "Auger Recombination in Chemical Vapor Deposition-Grown Monolayer WS2," J. Phys. Chem. Lett. **7**(24), 5242–5246 (2016).
23. F. Nan, Y.-H. Qiu, L. Zhou, and Q.-Q. Wang, "Ultrafast exciton dynamics in chemical heterogenous WSe2 monolayer," J. Phys. D: Appl. Phys. **50**(48), 485109 (2017).
24. E. J. Sie, A. Steinhoff, C. Gies, C. H. Lui, Q. Ma, M. Rosner, G. Schonhoff, F. Jahnke, T. O. Wehling, Y. H. Lee, J. Kong, P. Jarillo-Herrero, and N. Gedik, "Observation of Exciton Redshift-Blueshift Crossover in Monolayer WS2," Nano Lett. **17**(7), 4210–4216 (2017).
25. T. Jiang, R. Chen, X. Zheng, Z. Xu, and Y. Tang, "Photo-induced excitonic structure renormalization and broadband absorption in monolayer tungsten disulphide," Opt. Express **26**(2), 859–869 (2018).
26. J. Kim, X. Hong, C. Jin, S.-F. Shi, C.-Y. S. Chang, M.-H. Chiu, L.-J. Li, and F. Wang, "Ultrafast generation of pseudo-magnetic field for valley excitons in WSe2 monolayers," Science **346**(6214), 1205–1208 (2014).
27. E. J. Sie, J. W. McIver, Y. H. Lee, L. Fu, J. Kong, and N. Gedik, "Valley-selective optical Stark effect in monolayer WS2," Nat. Mater. **14**(3), 290–294 (2015).
28. E. J. Sie, C. H. Lui, Y. H. Lee, J. Kong, and N. Gedik, "Observation of Intervalley Biexcitonic Optical Stark Effect in Monolayer WS2," Nano Lett. **16**(12), 7421–7426 (2016).
29. C. Ruppert, A. Chernikov, H. M. Hill, A. F. Rigosi, and T. F. Heinz, "The Role of Electronic and Phononic Excitation in the Optical Response of Monolayer WS2 after Ultrafast Excitation," Nano Lett. **17**(2), 644–651 (2017).
30. T. O. Kwangu Kang, D. G. Cahill, and M. Shim, "Optical Phonon Lifetimes in Single-Walled Carbon Nanotubes by Time-Resolved Raman Scattering," Nano Lett. **8**(12), 4642–4647 (2008).
31. D. Song, F. Wang, G. Dukovic, M. Zheng, E. D. Semke, L. E. Brus, and T. F. Heinz, "Direct measurement of the lifetime of optical phonons in single-walled carbon nanotubes," Phys. Rev. Lett. **100**(22), 225503 (2008).
32. R. P. Saichu, I. Mahns, A. Goos, S. Binder, P. May, S. G. Singer, B. Schulz, A. Rusydi, J. Unterhinninghofen, D. Manske, P. Guptasarma, M. S. Williamsen, and M. Rubhausen, "Two-component dynamics of the order parameter of high temperature Bi2Sr2CaCu2O8 + delta superconductors revealed by time-resolved Raman scattering," Phys. Rev. Lett. **102**(17), 177004 (2009).
33. H. Yan, D. Song, K. F. Mak, I. Chatzakis, J. Maultzsch, and T. F. Heinz, "Time-resolved Raman spectroscopy of optical phonons in graphite: Phonon anharmonic coupling and anomalous stiffening," Phys. Rev. B **80**(12), 121403 (2009).
34. J. M. Nesbitt and D. C. Smith, "Measurements of the population lifetime of D band and G' band phonons in single-walled carbon nanotubes," Nano Lett. **13**(2), 416–422 (2013).

Optics EXPRESS

35. J. Zhu, R. German, B. V. Senkovskiy, D. Haberer, F. R. Fischer, A. Gruneis, and P. H. M. van Loosdrecht, "Exciton and phonon dynamics in highly aligned 7-atom wide armchair graphene nanoribbons as seen by time-resolved spontaneous Raman scattering," Nanoscale **10**(37), 17975–17982 (2018).
36. Z. Q. Xu, Y. Zhang, S. Lin, C. Zheng, Y. L. Zhong, X. Xia, Z. Li, P. J. Sophia, M. S. Fuhrer, Y. B. Cheng, and Q. Bao, "Synthesis and Transfer of Large-Area Monolayer WS2 Crystals- Moving Toward the Recyclable Use of Sapphire Substrates," ACS Nano **9**(6), 6178–6187 (2015).
37. Q. Fu, W. Wang, L. Yang, J. Huang, J. Zhang, and B. Xiang, "Controllable synthesis of high quality monolayer WS2 on a SiO2/Si substrate by chemical vapor deposition," RSC Adv. **5**(21), 15795–15799 (2015).
38. R. B. Versteeg, J. Zhu, P. Padmanabhan, C. Boguschewski, R. German, M. Goedecke, P. Becker, and P. H. M. van Loosdrecht, "A tunable time-resolved spontaneous Raman spectroscopy setup for probing ultrafast collective excitation and quasiparticle dynamics in quantum materials," Struct. Dyn. **5**(4), 044301 (2018).
39. H. R. Gutierrez, N. Perea-Lopez, A. L. Elias, A. Berkdemir, B. Wang, R. Lv, F. Lopez-Urias, V. H. Crespi, H. Terrones, and M. Terrones, "Extraordinary room-temperature photoluminescence in triangular WS2 monolayers," Nano Lett. **13**(8), 3447–3454 (2013).
40. W. Zhao, Z. Ghorannevis, L. Chu, M. Toh, C. Kloc, P. H. Tan, and G. Eda, "Evolution of electronic structure in atomically thin sheets of WS2 and WSe2," ACS Nano **7**(1), 791–797 (2013).
41. A. A. Mitioglu, P. Plochocka, G. Deligeorgis, S. Anghel, L. Kulyuk, and D. K. Maude, "Second-order resonant Raman scattering in single-layer tungsten disulfideWS2," Phys. Rev. B **89**(24), 245442 (2014).
42. A. Berkdemir, H. R. Gutiérrez, A. R. Botello-Méndez, N. Perea-López, A. L. Elías, C.-I. Chia, B. Wang, V. H. Crespi, F. López-Urías, J.-C. Charlier, H. Terrones, and M. Terrones, "Identification of individual and few layers of WS2 using Raman Spectroscopy," Sci. Rep. **3**(1), 1755 (2013).
43. T. M. and D and J. Late, "Temperature dependent phonon shifts in single-layer WS2," ACS Appl. Mater. Interfaces **6**(2), 1158–1163 (2014).
44. M. Staiger, R. Gillen, N. Scheuschner, O. Ochedowski, F. Kampmann, M. Schleberger, C. Thomsen, and J. Maultzsch, "Splitting of monolayer out-of-planeA1′Raman mode in few-layerWS2," Phys. Rev. B **91**(19), 195419 (2015).
45. C. Lee, B. G. Jeong, S. J. Yun, Y. H. Lee, S. M. Lee, and M. S. Jeong, "Unveiling Defect-Related Raman Mode of Monolayer WS2 via Tip-Enhanced Resonance Raman Scattering," ACS Nano **12**(10), 9982–9990 (2018).
46. X. Zhang, X.-F. Qiao, W. Shi, J.-B. Wu, D.-S. Jiang, and P.-H. Tan, "ChemInform Abstract: Phonon and Raman Scattering of Two-Dimensional Transition Metal Dichalcogenides from Monolayer, Multilayer to Bulk Material," Chem. Soc. Rev. **44**(9), 2757–2785 (2015).
47. J. A. Kash, J. C. Tsang, and J. M. Hvam, "Sub-picosecond time-resolved Raman spectroscopy of LO phonons in GaAs," Phys. Rev. Lett. **54**(19), 2151–2154 (1985).
48. K. T. Tsen and H. Morkoç, "Subpicosecond time-resolved Raman spectroscopy of LO phonons in GaAs-AlxGa1−xAs multiple-quantum-well structures," Phys. Rev. B **38**(8), 5615–5616 (1988).
49. M. Baranowski, A. Surrente, D. K. Maude, M. Ballottin, A. A. Mitioglu, P. C. M. Christianen, Y. C. Kung, D. Dumcenco, A. Kis, and P. Plochocka, "Dark excitons and the elusive valley polarization in transition metal dichalcogenides," 2D Mater. **4**(2), 025016 (2017).
50. M. R. Molas, C. Faugeras, A. O. Slobodeniuk, K. Nogajewski, M. Bartos, D. M. Basko, and M. Potemski, "Brightening of dark excitons in monolayers of semiconducting transition metal dichalcogenides," 2D Mater. **4**(2), 021003 (2017).
51. K. P. Loh, "Brightening the dark excitons," Nat. Nanotechnol. **12**(9), 837–838 (2017).
52. M. Danovich, V. Zolyomi, and V. I. Fal'ko, "Dark trions and biexcitons in WS2 and WSe2 made bright by e-e scattering," Sci. Rep. **7**(1), 45998 (2017).
53. M. Van der Donck, M. Zarenia, and F. M. Peeters, "Strong valley Zeeman effect of dark excitons in monolayer transition metal dichalcogenides in a tilted magnetic field," Phys. Rev. B **97**(8), 081109 (2018).
54. Z. Wang, A. Molina-Sánchez, P. Altmann, D. Sangalli, D. De Fazio, G. Soavi, U. Sassi, F. Bottegoni, F. Ciccacci, and M. Finazzi, "Intravalley Spin–Flip Relaxation Dynamics in Single-Layer WS2," Nano Lett. **18**(11), 6882–6891 (2018).
55. V. Carozo, Y. Wang, K. Fujisawa, B. R. Carvalho, A. McCreary, S. Feng, Z. Lin, C. Zhou, N. Perea-Lopez, A. L. Elias, B. Kabius, V. H. Crespi, and M. Terrones, "Optical identification of sulfur vacancies: Bound excitons at the edges of monolayer tungsten disulfide," Sci. Adv. **3**(4), e1602813 (2017).
56. X. Liu, J. Hu, C. Yue, N. Della Fera, Y. Ling, Z. Mao, and J. Wei, "High performance field-effect transistor based on multilayer tungsten disulfide," ACS Nano **8**(10), 10396–10402 (2014).
57. L. Yuan, T. Wang, T. Zhu, M. Zhou, and L. Huang, "Exciton Dynamics, Transport, and Annihilation in Atomically Thin Two-Dimensional Semiconductors," J. Phys. Chem. Lett. **8**(14), 3371–3379 (2017).
58. E. Nurfani, R. Kurniawan, T. Aono, K. Takeda, Y. Shirai, I. M. Sutjahja, A. Rusydi, T. Winata, K. Takase, and Y. Darma, "Defect-induced excitonic recombination in Ti x Zn1− x O thin films grown by DC-unbalanced magnetron sputtering," Jpn. J. Appl. Phys. **56**(11), 112101 (2017).
59. K. R. Reid, J. R. McBride, A. D. La Croix, N. J. Freymeyer, S. M. Click, J. E. Macdonald, and S. J. Rosenthal, "Role of Surface Morphology on Exciton Recombination in Single Quantum Dot-in-Rods Revealed by Optical and Atomic Structure Correlation," ACS Nano **12**(11), 11434–11445 (2018).
60. R. Loudon, "The Raman effect in crystals," Adv. Phys. **13**(52), 423–482 (1964).

Optics EXPRESS

61. J. Zhu, R. B. Versteeg, P. Padmanabhan, and P. H. M. van Loosdrecht, "Dynamical resonance quench and Fano interference in spontaneous Raman scattering from quasiparticle and collective excitations," Phys. Rev. B **99**(9), 094305 (2019).